Received: 24 January 2022 | Revised: 2 March 2022 | Accepted: 2 March 2022

DOI: 10.1002/cjce.24410

SPECIAL ISSUE ARTICLE

THE CANADIAN JOURNAL OF CHEMICAL ENGINEERING

Liquid co-fluidization of cylinders and spheres

Jacobus J. Derksen

School of Engineering, University of Aberdeen, Aberdeen, UK

Correspondence
Jacobus J. Derksen, School of Engineering, University of Aberdeen, Aberdeen, UK.
Email: jderksen@abdn.ac.uk

Abstract

Liquid fluidization of mixtures of solid particles of spherical and cylindrical shape has been numerically simulated. The simulations explicitly resolve the solid–liquid interfaces by means of an immersed boundary method implemented in a lattice-Boltzmann flow solver. A soft collision algorithm deals with particle–particle contacts and close-range hydrodynamic interaction. The systems studied have an overall solids volume fraction of 0.40, with 5%–35% of the overall solids volume contained in the cylinders. One focus of the study is on the effect of the length over diameter aspect ratio (that has been varied between 4–10) of the cylinders on the co-fluidization behaviour. The average slip velocity of the cylinders only weakly depends on the fraction of the cylinder volume in the solid particle mixture. The cylinders do stir the system, with velocity fluctuation levels increasing if the number of cylinders relative to the number of spheres is increased. When co-fluidized, the taller cylinders preferentially orient vertically, as they also do in cylinder-only fluidization.

KEYWORDS

lattice-Boltzmann method, liquid fluidization, non-spherical particles, particle-resolved simulation

1 | INTRODUCTION

Processing of dense fluid–solid mixtures is commonplace in many industrial processes. For this reason, the fluid dynamics of suspensions is a topic of considerable societal and economic relevance. Control over suspension transport phenomena enables the design and optimization of industrial processes. In light of this, considerable research effort is directed towards developing computational methodologies for predicting the behaviour of multiphase flow systems. The overarching challenge is the multi-scale nature of multiphase flow that has a large disparity in length scales. For fluid–solid systems—the topic of this paper—length scales range from equipment size (of the order of metres) to particle size (anywhere between hundreds of nanometres and millimetres), not to speak of the length-scales associated with the particle surfaces (such as roughness). Capturing the full spectrum of length scales (and associated time scales) in a comprehensive computer simulation is currently impossible and will be so in the foreseeable future.

For this reason, computer simulations of industrial-scale multiphase transport processes use closure models to account for the effect particle-scale phenomena have on macroscopic behaviour.[1] Such models involve detailed notions as to how solid particles dynamically

interact with the surrounding fluid. These notions have been obtained through theory,[2] experiment,[3] as well as simulation.[4] This paper further explores the latter aspect: by performing detailed, particle-resolved, microscopic simulations, we probe dynamic solid–liquid interactions. We specifically (and explicitly) involve particle shape in our work. Most of the models for solid–fluid interactions are based on particles being spherical, or at least sufficiently spherical, so as to apply what is known as drag forces on single spheres and sphere assemblies. We introduce cylindrical particles in the micro-scale simulations. This is because of the practical relevance of fibre suspensions in, for instance, paper pulp processing or biomass conversion. It is also because cylinders with circular cross-sections have only one aspect ratio (length over diameter ℓ/d) so that particle shape effects are controlled by only one dimensionless parameter.

The micro-scale simulations presented here are of fluidized systems in fully periodic, three-dimensional domains with the particles freely moving under the influence of fluid flow, gravity, and particle–particle interactions. We have performed such simulations previously for spheres,[5] rigid cylinders,[6] and flexible cylinders[7] with the aim of quantifying solid–fluid drag, (collisional) stress, the evolution of particle microstructure, and (for cylinders) the way they orient themselves relative to the direction of gravity. In the current paper, we study mixtures of spheres and cylinders. This choice has been instigated by previous experimental and computational studies on the co-fluidization of cylinders.[8–11] In an attempt to improve the fluidization behaviour of cylindrical particles, they are mixed with particles of a (more) spherical shape.

The aim of this paper is to provide a detailed look into the liquid fluidization of mixtures of cylinders and spheres through particle-resolved simulation. The focus is on liquid–solid systems (rather than gas–solid) with a view to our interest in bagasse (fibre-pulp biomass) processing.[12] We are not only interested in average fluidization (i.e., slip) velocities but also in particle velocity fluctuations as these are relevant in applications that involve solid–liquid mass transfer. The orientation of the cylinders relative to gravity is another point of attention. In simulations of dense cylinders-only fluidization, we noted a very strong preference for vertical orientation of the cylinders,[7] in qualitative agreement with experimental work.[13,14] The orientation preference of cylinders might be a reason for their poor fluidization characteristics.

This paper has been organized as follows: the next section defines the flow geometry and process conditions, mostly in terms of dimensionless numbers. We then briefly summarize the numerical procedures. They have been documented in previous papers in full detail, the novelty being that now we combine particles of spherical and cylindrical shape in a single simulation. It then is explained how the flow systems develop to a dynamically steady state. Statistical analyses of data collected during steady state are the core of Section 5. In this section, we also compare co-fluidized systems with cylinder-only fluidization. The final section reiterates the main conclusions of the work.

2 | FLOW SYSTEMS

The three-dimensional flow domains are rectangular, with size $nx \cdot ny \cdot nz$, and have fully periodic boundary conditions. They contain a Newtonian fluid that has density ρ and kinematic viscosity ν, and rigid solid particles in the form of identical spheres and identical cylinders with an overall solids volume fraction $\langle\phi\rangle$. The spheres have diameter a d, and the cylinders have a length ℓ and a diameter d (i.e., their diameter is equal to the diameter of the spheres). The main dependencies we will be investigating are the aspect ratio of the cylinders ℓ/d that has been varied in the range of 4–10 and the solids volume contained in the cylinders relative to the total solids volume that has been varied from $\langle\phi_c\rangle/\langle\phi\rangle = 0.05$–$0.35$ (with $\langle\phi_c\rangle$ being the volume fraction of cylinders). All solids have the same density ρ_p such that the density ratio $\gamma = \rho_p/\rho = 2.0$; this is a value typical for a solid–liquid system.

Gravity points in the negative z-direction: $\mathbf{g} = -g\mathbf{e_z}$. Since we have fully periodic boundary conditions, we need to explicitly balance forces over the entire system. This is achieved by compensating the net gravity acting on the particles in the negative z-direction with a body force $\mathbf{f}$ acting on the fluid in the positive z-direction $\mathbf{f} = \rho\langle\phi\rangle(\gamma-1)g\mathbf{e_z}$.[5] Gravity and density ratio are combined in the Archimedes number $\mathrm{Ar} = (\gamma-1)gd^3/\nu^2$ that has been set at $\mathrm{Ar} = 864$. The choice of using d as the length scale in Ar is because this is the length scale shared by all particles—spheres and cylinders—in the simulations. The overall solids volume fraction in this study has been fixed to $\langle\phi\rangle = 0.40$.

3 | NUMERICAL PROCEDURES

The fluid flow is solved by the means of the lattice-Boltzmann (LB) method,[15] specifically the scheme proposed by Somers.[16,17] It operates on a uniform cubic grid with spacing Δ and evolves in time with a time step Δt. The spatial resolution is such that $d = 16\Delta$, and the

temporal resolution is such that the viscous time scale $d^2/\nu = 6400\Delta t$. Grid and time step convergence studies have been discussed in previous work.[6] At Archimedes numbers comparable as to the one in that paper, differences in average hindered settling speeds between $d = 16\Delta$ and $d = 24\Delta$ are within 1%.[6]

An immersed boundary method (IBM) has been used to represent the surfaces of solid particles.[18] These surfaces are covered with marker points that have a nearest neighbour spacing in the range of $0.5\Delta - 0.7\Delta$. At the marker points, the fluid is forced to the same velocity as the velocity of the solid surface so as to achieve no-slip. The force distribution over the solid surface of each particle is integrated to determine the hydrodynamic force and torque acting on the particle. Along with the contact forces and their resulting torques (see below) and net gravity, the hydrodynamic forces, and torques are used to update the linear and rotational equations of motion of each particle so as to determine their linear and angular velocity. Updating the orientation of the particles makes use of quaternions.[19,20] Particle updates as described above use the same time step Δt as the LB updates.

The final element of the simulation procedure is collision handling. The IBM marker points are also instrumental in this respect. If two marker points on two different particles get into close proximity, a contact force between them is activated. The contact force has two elements: (1) a linear elastic repulsive force that mimics direct (solid–solid) contact between particles and (2) a force that depends on the relative velocity between the marker points that mimics lubrication. The expressions for the contact force have been given in full detail in previous work.[6] The contact force coefficients used in that paper are identical to the ones used in the current paper.

4 | SET-UP OF SIMULATIONS

The particles are placed in a non-overlapping manner in the $nx \cdot ny \cdot nz$ fully periodic flow domain. The default domain size is $15d \cdot 15d \cdot 30d$. Domain size effects have been assessed previously[6] and also in this paper for one case that had a domain of volume $12d \cdot 12d \cdot 24d$ and contained $\ell/d = 10$ cylinders. These are the tallest cylinders studied for which domain size effects are expected to be most critical. Initially, fluid and particles are at rest.

Examples of the way the systems develop are illustrated in Figures 1 and 2. Figure 1 shows the time series of the Reynolds number per particle type,

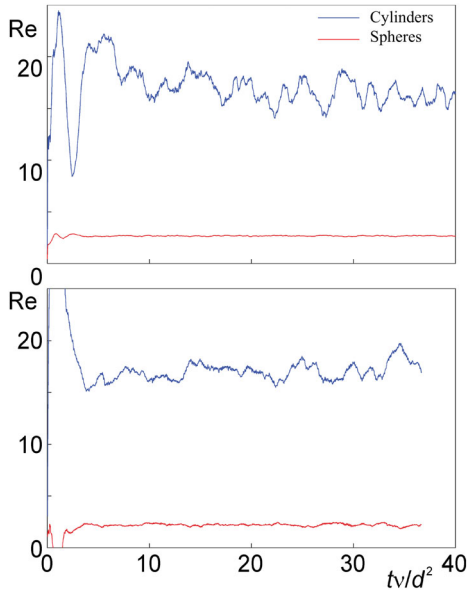

FIGURE 1 Time series of Re based on the slip velocity between fluid and particles for cylinders and spheres as indicated. The cylinders have an aspect ratio $\ell/d = 8$. Top panel: 5% of solids volume is in the cylinders ($\langle\phi_c\rangle/\langle\phi\rangle = 0.05$) and bottom panel: $\langle\phi_c\rangle/\langle\phi\rangle = 0.35$

defined as $\mathrm{Re} = \frac{|\langle u_z\rangle - \langle u_{pz}\rangle| d_e}{\nu}$ with $\langle u_z\rangle$ the volume-averaged superficial fluid velocity in the z-direction, $\langle u_{pz}\rangle$ the volume-averaged particle velocity in the z-direction, and d_e the equivalent particle diameter ($d_e = d$ for the spheres and $d_e = d\sqrt[3]{\frac{3}{2}\ell/d}$ for the cylinders). In Figure 1, we distinguish between the Reynolds numbers of spheres and cylinders. In the top panel of Figure 1, the fluctuations of the Reynolds number of the cylinders are much larger than those of the spheres, simply because there are many more spheres than cylinders (4899 spheres and 21 cylinders). The spheres quickly establish a (dynamically) steady value for their Reynolds number. Reaching a dynamically steady Reynolds number takes much longer for the cylinders. The reason for the latter is illustrated in the top row panels of Figure 2 that show instantaneous realizations of particle configurations for $\langle\phi_c\rangle/\langle\phi\rangle = 0.05$. The cylinders need time to orient themselves and to spread evenly over the flow domain. For instance, as shown in Figure 2, at $t\nu/d^2 = 3.13$ the cylinders tend to prefer to be on one side of the domain. After $t\nu/d^2 \approx 20$, the cylinder Reynolds number fluctuates around a stable value.

Figure 2 also shows examples of how a system with $\langle\phi_c\rangle/\langle\phi\rangle = 0.35$ was initialized. As can be seen in Figure 1, this results, for the cylinders, in very strong Reynolds number fluctuations at the start of the simulation.

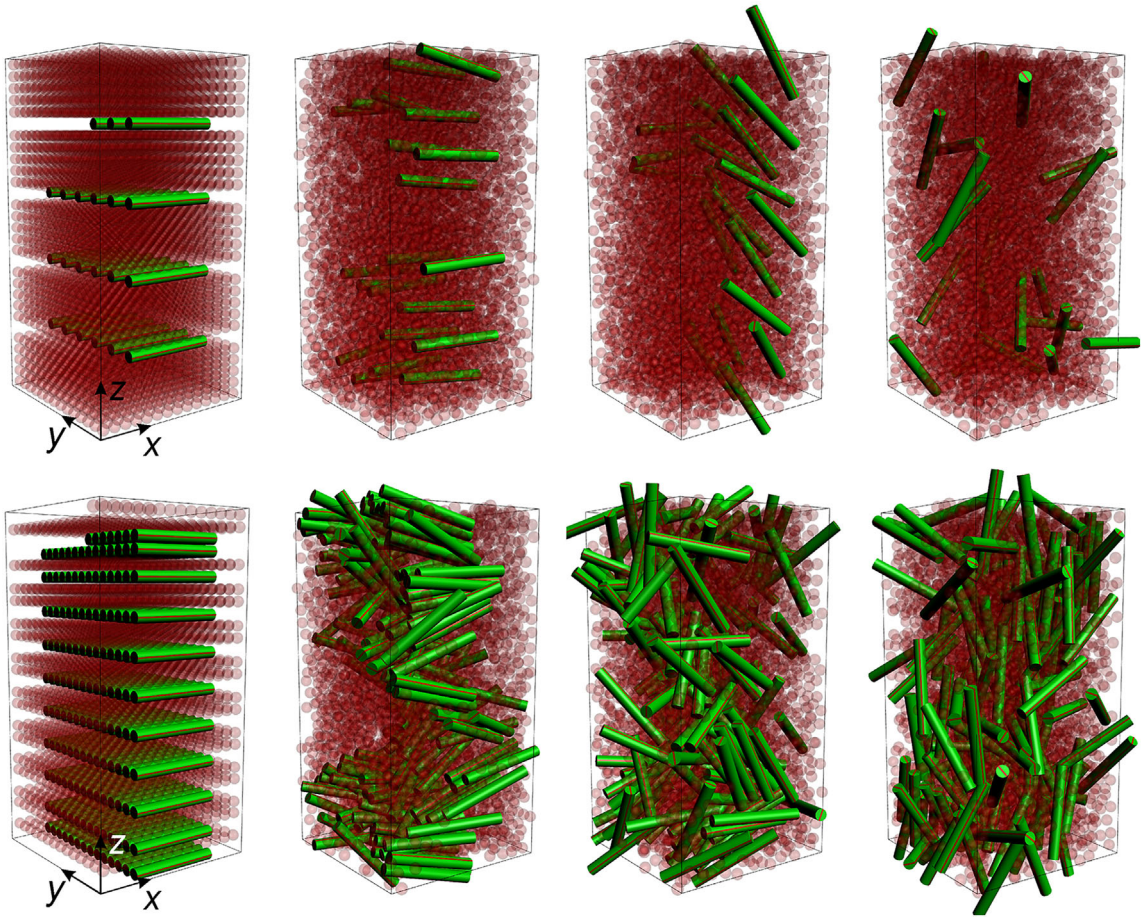

FIGURE 2 Instantaneous realizations of particles: spheres and cylinders with $\ell/d = 8$. Top row: 5% of the solids volume is in the cylinders and bottom row: 35% of the solids volume is in the cylinders. From left to right $t\nu/d^2 = 0,\ 1.56,\ 3.13,\ 36.7$. The spheres have been made semi-transparent to allow us to see (most of) the cylinders

In order to have sufficient data for meaningful statistical analysis over a quasi-steady time window, all simulations reported have run until at least to $td^2/\nu = 35$.

5 | RESULTS

After the time series, such as the ones in Figure 1, indicate that a dynamically steady state has set in, we use data collected over the remainder of the simulation time to perform statistical analyses. The Reynolds number data in Figure 1 is an average over the flow volume as a function of time. Also, averaging over time provides double averaged (time and volume) Reynolds numbers. These are presented in Figure 3 for all cases considered. As for cylinder-only fluidization,[6] the Reynolds number increases with an increasing aspect ratio ℓ/d. It is quite remarkable to see that the Reynolds number of the cylinders (top panel of Figure 3) does not significantly depend on the relative amount of cylinder volume, expressed as $\langle\phi_c\rangle/\langle\phi\rangle$. For $\ell/d < 10$, these constant levels of Re, and thus the cylinder slip velocities, are slightly higher than for fluidization of cylinders only at an overall solids volume fraction of $\langle\phi\rangle = 0.40$ (indicated by the dashed lines in Figure 3 that are data from previous works[6,7]).

The lower panel of Figure 3 indicates that the spheres slightly slow down if the solids volume contained in the cylinders increases. That effect does not exhibit a clear trend in terms of the aspect ratio of the cylinders the sphere is mixed with.

Figure 3 might suggest that (at least up to $\langle\phi_c\rangle/\langle\phi\rangle = 0.35$) the cylinders hardly interact with one another given that their average speed is independent of $\langle\phi_c\rangle/\langle\phi\rangle$. As we see in Figure 4, however, there is a marked effect of $\langle\phi_c\rangle/\langle\phi\rangle$ on the fluctuating velocity of the cylinders. The Reynolds number, associated with the particle velocity fluctuations, is defined as $\mathrm{Re}_{rms,\alpha} = d_e\sqrt{\overline{\left(u_{p\alpha} - \langle u_{p\alpha}\rangle\right)^2}}/\nu$ where α indicates the coordinate direction. The time average involved in determining $\mathrm{Re}_{rms,\alpha}$ is over a time window after the flow system has become dynamically steady.

THE CANADIAN JOURNAL OF CHEMICAL ENGINEERING

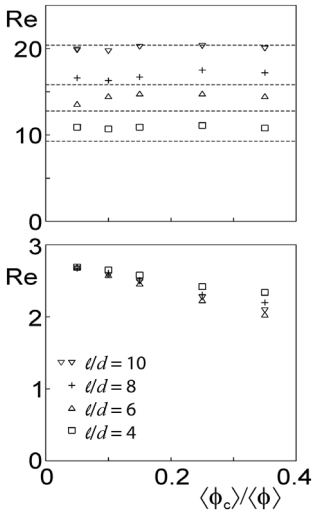

FIGURE 3 Time and volume average slip velocity Reynolds number as a function $\langle\phi_c\rangle/\langle\phi\rangle$ (the fraction of solids volume contained in cylinders relative to the total solids volume) for various aspect ratios of the cylinders ℓ/d as indicated. Top panel: Reynolds number for the cylinders and bottom panel: Reynolds number for the spheres. The dashed horizontal lines in the top panel indicate Re for cylinder-only fluidization at $\langle\phi\rangle = 0.40$[6,7] for (from top to bottom) $\ell/d = 10$, 8, 6, and 4, respectively. The blue symbol is for a smaller domain size (see text)

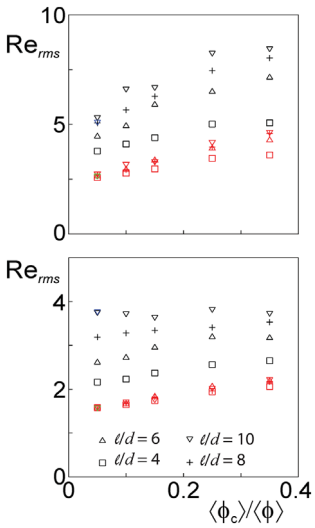

FIGURE 4 Time and volume average Reynolds number associated with particle velocity fluctuations (Re_{rms}) as a function $\langle\phi_c\rangle/\langle\phi\rangle$. Cases with various ℓ/d as indicated. Black symbols relate to cylinders' velocity fluctuations, whereas red symbols relate to spheres' velocity fluctuations. The blue and green symbols are for a smaller domain. Top panel: fluctuations in vertical direction and bottom: fluctuations in the horizontal direction

There are a few observations to be made in Figure 4. (1) Velocity fluctuation levels in vertical as well as in horizontal direction increase with the length of the cylinders. (2) Vertical velocity fluctuations of the cylinders as well as of the spheres increase with increasing $\langle\phi_c\rangle/\langle\phi\rangle$.

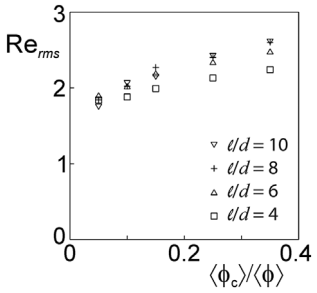

FIGURE 5 Time and volume average Reynolds number associated with cylinder rotation fluctuations Re_{rot} (definition, see text) as a function $\langle\phi_c\rangle/\langle\phi\rangle$. Cases with various ℓ/d as indicated

(3) Horizontal velocity fluctuations do not show a consistent trend with $\langle\phi_c\rangle/\langle\phi\rangle$. (4) Velocity fluctuations in the vertical direction are systematically stronger than in the horizontal direction. (5) The velocity fluctuations of the spheres barely depend on the aspect ratio of the cylinder they are mixed with.

The increasing vertical fluctuation levels with increasing $\langle\phi_c\rangle/\langle\phi\rangle$ imply that the cylinders tend to agitate the system (fluid, spheres, and cylinders). Why this only shows in the vertical direction is not directly clear. The fluidization velocity fluctuations are stronger in the direction of gravity than in the lateral direction; this concept has earlier been established for fluidization of spheres[5] and of cylinders[6,7] separately and now thus also for mixtures of spheres and cylinders.

Figures 3 and 4 contain additional data points for a domain smaller than the default domain for the case with $\langle\phi_c\rangle/\langle\phi\rangle = 0.05$ and $\ell/d = 10$ (see Section 4 for the respective domain sizes). It can be observed that there are only marginal differences between the results obtained in the two domains. Given that this condition is for the tallest cylinders, we are confident that, overall, the results presented do not depend significantly on our choice of domain size.

Relative motion between fluid and cylinders is not only the result of linear velocities, but also of angular velocities of the cylinders. In order to estimate the relative strength of the rotational fluid–solid slip of the cylinders, we determine a root-mean-square rotational Reynolds number $Re_{rot} = d_e\sqrt{\overline{\left(\omega_{p2}^2 + \omega_{p3}^2\right)}}\frac{\ell}{2}/\nu$ with ω_{p2} and ω_{p3} angular velocities about principal axes 2 and 3 (principal axis 1 being the centre line) of the cylinder. The results in Figure 5 show that Re_{rot} is comparable to Re_{rms} of the horizontal linear velocities (lower panel of Figure 4) and significantly smaller than Re_{rms} of the vertical linear velocities. Interestingly, Re_{rot} only weakly depends on ℓ/d, at least for $\langle\phi_c\rangle/\langle\phi\rangle \leq 0.15$. Since Re_{rot} is proportional to ℓ, this implies higher rotation rates for shorter cylinders.

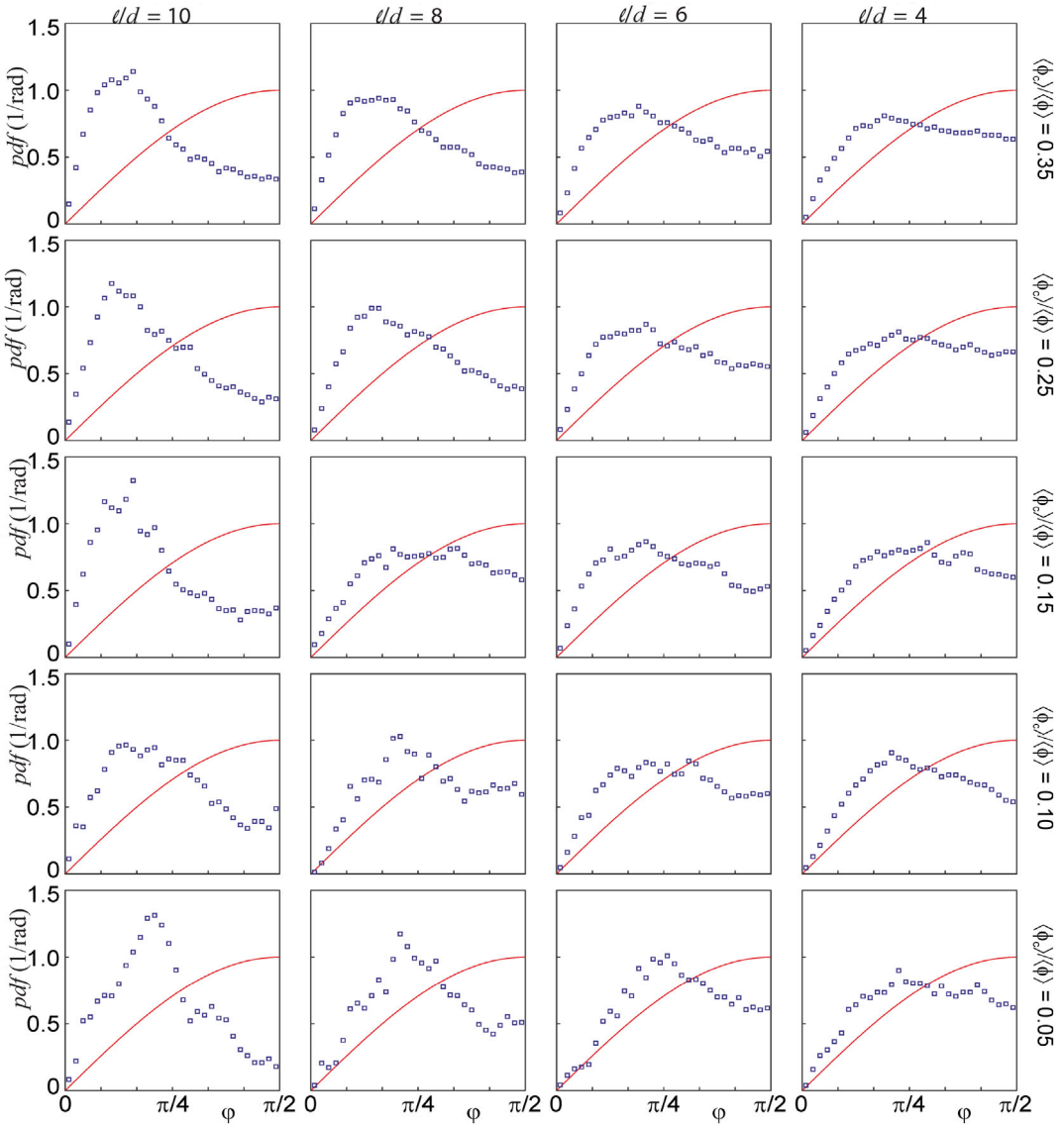

FIGURE 6 Probability density functions (pdfs) of the angle φ of the cylinders with the vertical for simulations with (from left to right) decreasing ℓ/d and (from top to bottom) decreasing $\langle\phi_c\rangle/\langle\phi\rangle$. Symbols are simulation results, and the red curve is $\sin\varphi$

In dense fluidized cylinder-only suspensions, tall cylinders prefer to orient vertically.[7,13] The shorter the cylinders or the lower the solids volume fraction, the weaker this preferential orientation becomes.[6] In that light, it is relevant to investigate the orientation preference of cylinders when co-fluidized with spheres. Cylinder orientation has been quantified by the distribution of the angle φ between the centre line of the cylinder and the vertical direction; $\varphi = 0$ is vertical, $\varphi = \pi/2$ horizontal. An isotropic distribution of orientations has a φ-distribution according to $\sin\varphi$. Figure 6 shows the orientation angle distributions for all cases considered in this paper. Comparison between the $\sin\varphi$ distribution and the simulated distributions teaches us that in all these cases, the cylinders tend to be fluidized with the small angles being over-represented and the large angles under-represented. This effect is strongest for the tallest ($\ell/d = 10$) cylinders and weakest for the (shortest) $\ell/d = 4$ cylinders. For $\ell/d = 10$, it is surprising that the preference for small angles with the vertical is observed to be approximately of the same extent over the entire range of $\langle\phi_c\rangle/\langle\phi\rangle$ investigated. One could expect that the presence of spheres would randomize the cylinder orientation so that the more spheres (i.e., the lower $\langle\phi_c\rangle/\langle\phi\rangle$), the more isotropic the φ distribution. In Figure 6, this effect can be identified for $\ell/d \leq 8$, but not for $\ell/d = 10$.

It is meaningful to compare co-fluidization of sphere-cylinder mixtures with the fluidization of only cylinders. Results from simulations of the latter systems have been previously published.[6,7] The comparison

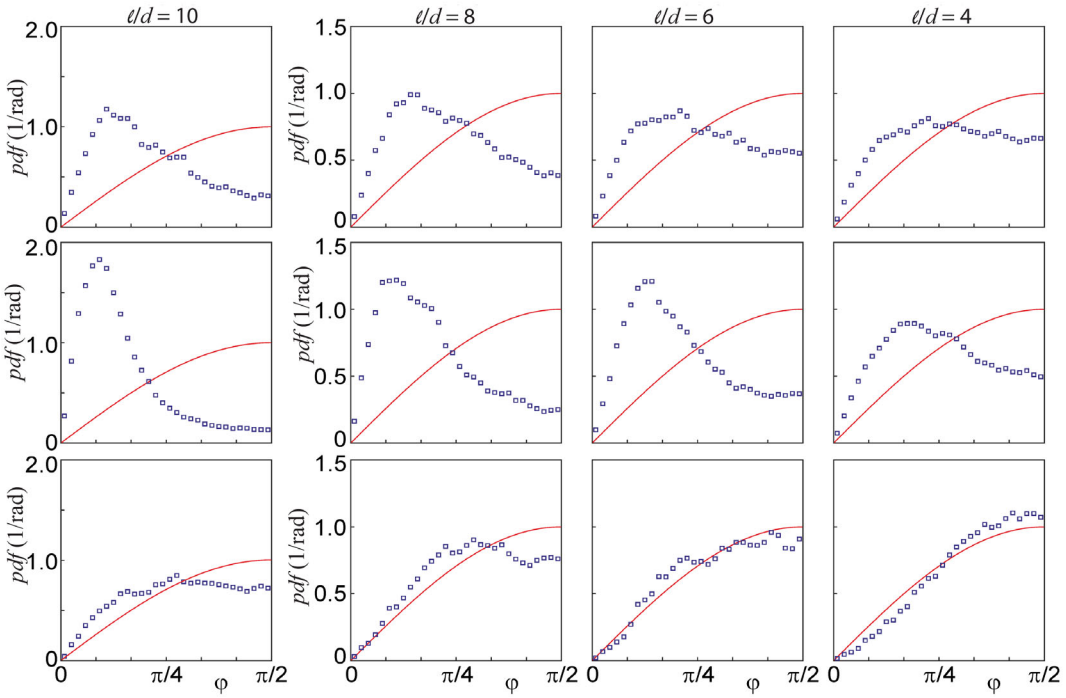

FIGURE 7 Probability density functions (pdfs) of the angle φ of the cylinders with the vertical for simulations with (from left to right) decreasing ℓ/d. Top row: co-fluidized systems with $\langle\phi_c\rangle/\langle\phi\rangle = 0.25$ (and $\langle\phi\rangle = 0.40$). Middle row: cylinders only with $\langle\phi\rangle = 0.40$.[7] Bottom row: cylinders only with $\langle\phi\rangle = 0.10$.[7] Symbols are simulation results, and the red curve is $\sin\varphi$

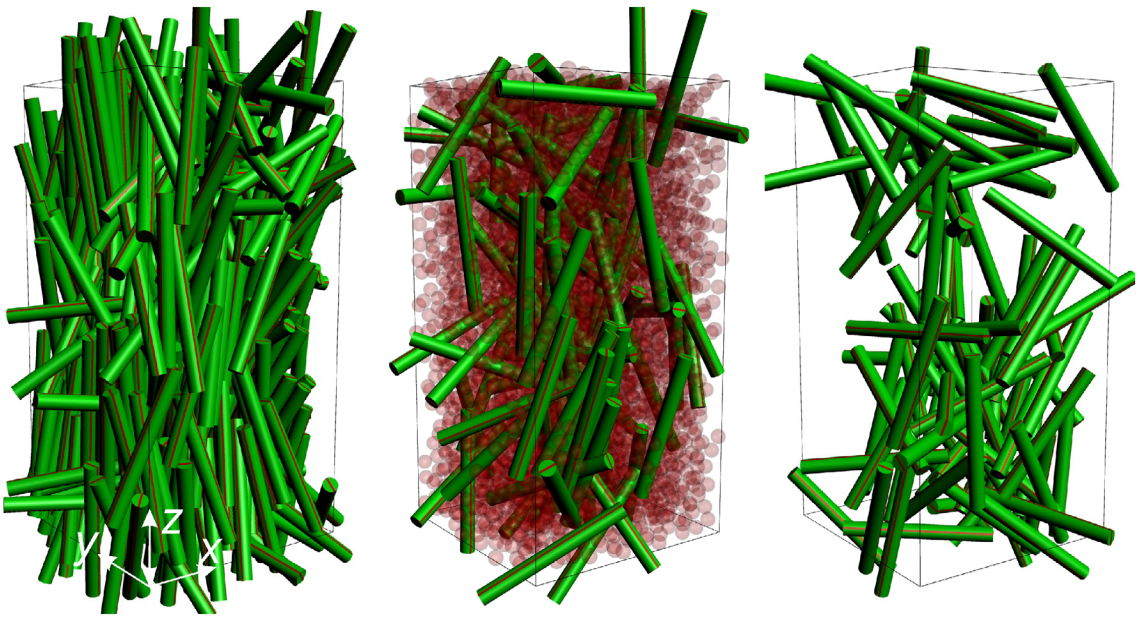

FIGURE 8 Instantaneous realizations of cylinder-only fluidization (from left to right) with $\langle\phi\rangle = 0.40$, co-fluidization with $\langle\phi_c\rangle/\langle\phi\rangle = 0.25$ and $\langle\phi\rangle = 0.40$, and cylinder-only fluidization with $\langle\phi\rangle = 0.10$. In all three cases, $\ell/d = 10$

is shown in Figure 7 in terms of orientation angle distributions with a focus on the co-fluidized systems with $\langle\phi_c\rangle/\langle\phi\rangle = 0.25$ that have an overall solids volume fraction of $\langle\phi\rangle = 0.40$. We compare these results with—on one side—only-cylinder simulations with $\langle\phi\rangle = 0.40$, and—on the other side—only-cylinder simulations with $\langle\phi\rangle = 0.10$, the latter because this is equal to $\langle\phi_c\rangle$ of the co-fluidized cases.

As we see in Figure 7, the $\langle\phi\rangle = 0.40$ cases with only cylinders have a strong (very strong for $\ell/d = 10$)

preference for vertical orientation; the cases with $\langle\phi\rangle = 0.10$ are to a fair approximation, isotropic. The co-fluidized cases are in between these two "extremes". Given the isotropy of spheres, one could have expected the co-fluidized cases to be closer to the isotropic ($\langle\phi\rangle = 0.10$) cases. The opposite is true: at least for $\ell/d < 10$, the co-fluidized angle distributions are much closer to the $\langle\phi\rangle = 0.40$ cylinder-only distributions than to the $\langle\phi\rangle = 0.10$ cylinder-only distributions. Apparently, the interstitial spheres play a role in communicating the preference for the smaller orientation angles among the co-fluidized cylinders. Figure 8 provides anecdotal evidence for the distributions for $\ell/d = 10$, as shown in Figure 7, and some qualitative insight into how the cylinders orient themselves.

6 | CONCLUSIONS

This paper reports on particle-resolved simulations of co-fluidization of cylinders and spheres with all solids having the same density. The solid–fluid density ratio $\gamma = 2$ is representative of liquid–solid systems. The flow systems are tri-periodic, mimicking a small sample in a much larger fluidized bed away from walls or internal structures. Results have mostly been presented in statistical form—as averages and distributions—from data collected over a period of steady fluidization. All cases considered have the same Archimedes number and the same overall solids volume fraction. The dependencies investigated were the aspect ratio of the cylinders and the amount of volume contained in the cylinders, keeping the overall solids volume constant.

The average superficial slip velocity of cylinders of equal length appears to be independent of the amount of cylinder volume present, while longer cylinders have higher slip velocities than shorter ones. The latter is simply because, under the conditions, we investigated that the net gravity force is higher on longer cylinders. The strength of the velocity fluctuations of the cylinders in the vertical direction does positively correlate with the relative amount of cylinder volume. As for other fluidized systems, horizontal particle velocity fluctuations are significantly weaker than their vertical counterparts. Cylinder rotation contributes non-negligibly to slip (relative velocity) between fluid and solids.

In all cases considered in this study, the cylinders display a preference for orienting themselves with a relatively small angle with the vertical direction. This effect is more pronounced for longer cylinders. The distribution of angles is not a pronounced function of the relative numbers of cylinders, which is remarkable.

In order to progress in this line of research, first and foremost, there is a need for experimental data, not only for validation of the simulations but also for guidance of the simulations. It should be noted that in this paper, we only explored a relatively small part of the very large parameter space of co-fluidization. We have kept the overall volume fraction, Archimedes number, and solid–liquid density ratio constant and have spheres and cylinders with the same density and same diameter. Guidance from experiments and practical applications is needed to be able to zoom in on relevant regions of the parameter space. However, the paper has demonstrated the feasibility of detailed simulations of co-fluidizing systems and the type of information that can be extracted from them.

PEER REVIEW

The peer review history for this article is available at https://publons.com/publon/10.1002/cjce.24410.

DATA AVAILABILITY STATEMENT

Data available on request from the authors

AUTHOR CONTRIBUTIONS

Jacobus J. Derksen: Conceptualization; formal analysis; investigation; methodology; visualization; writing – original draft; writing – review & editing.

REFERENCES

[1] R. Jackson, *Chem. Eng. Sci.* **1997**, *52*, 2457.
[2] G. G. Stokes, *Mathematical and Physical Papers, Vol. I–V*, Cambridge University Press, Cambridge, UK **1901**.
[3] J. F. Richardson, W. N. Zaki, *Trans. Inst. Chem. Eng.* **1954**, *32*, 35.
[4] M. A. Van der Hoef, R. Beetstra, J. A. M. Kuipers, *J. Fluid Mech.* **2005**, *528*, 233.
[5] J. J. Derksen, S. Sundaresan, *J. Fluid Mech.* **2007**, *587*, 303.
[6] J. J. Derksen, *AIChE J.* **2019**, *65*, pe16594.
[7] J. J. Derksen, *Acta Mech.* **2020**, *231*, 5193.
[8] L. Lu, J. Yu, X. Gao, Y. Xu, M. Shahnam, W. A. Rogers, *AIChE J.* **2020**, *66*, e16969.
[9] F. Fotovat, A. Abbasi, R. J. Spiteri, H. de Lasa, J. Chaouki, *Powder Technol.* **2015**, *275*, 39.
[10] X. Chen, W. Zhong, T. J. Heindel, *AIChE J.* **2019**, *65*, 520.
[11] F. Fotovat, R. Ansart, M. Hemati, O. Simonin, J. Chaouki, *Chem. Eng. Sci.* **2015**, *126*, 543.
[12] M. Inyang, B. Gao, P. Pullammanappallil, W. Ding, A. R. Zimmerman, *Bioresource Technol.* **2010**, *101*, 8868.
[13] B. Herzhaft, E. Guazzelli, *J. Fluid Mech.* **1999**, *384*, 133.
[14] B. Metzger, J. E. Butler, E. Guazzelli, *J. Fluid Mech.* **2007**, *575*, 307.
[15] S. Succi, *The Lattice Boltzmann Equation for Fluid Dynamics and Beyond*, Clarendon Press, Oxford, UK **2001**.
[16] J. A. Somers, *Appl. Sci. Res.* **1993**, *51*, 127.
[17] J. G. M. Eggels, J. A. Somers, *Int. J. Heat Fluid Fl.* **1995**, *16*, 357.
[18] A. Ten Cate, C. H. Nieuwstad, J. J. Derksen, H. E. A. van den Akker, *Phys. Fluids* **2002**, *14*, 4012.
[19] J. B. Kuipers, *Quaternions and Rotation Sequences*, Princeton University Press, Princeton, NJ **1999**.
[20] W. F. J. Phillips, C. E. Hailey, G. A. Gebert, *J. Aircraft* **2001**, *38*, 718.

AUTHOR BIOGRAPHY

Jacobus J. Derksen was educated in the Netherlands where he obtained a PhD degree in Applied Physics from Eindhoven University of Technology in 1991. After a short period with the Dutch Aerospace Laboratory (NLR) he joined Delft University of Technology in 1992. In 2007 he moved to the University of Alberta, Canada. In 2013 he came back to Europe to work with the University of Aberdeen (UK) and—in 2014/2015—Delft University. His research focuses on highly resolved simulations of multiphase flow and transport processes. [Correction added on 2 August 2022, after first online publication: the author name Jacobus J. Derksen was incorrect in the original published article and has been corrected in this version.]

How to cite this article: J. J. Derksen, *Can. J. Chem. Eng.* **2022**, *100*(9), 2623. https://doi.org/10.1002/cjce.24410